Impurity-Related Optical Response in Quantum Ring with Magnetic Field

Kang Yun and Wang Sheng*

School of Physics and Electronic Engineering, Northeast Petroleum University, No. 99 Xuefu Street, 163318, Daqing, China

Received: 17.02.2022 & Accepted: 30.05.2022

Doi: 10.12693/APhysPolA.142.242 *e-mail: wangsheng10@126.com

The optical absorption of the donor impurity in the two-dimensional GaAs quantum ring was studied with the effective mass approximation using the finite element method. The influence of the magnetic field, light intensity, and impurity position on the optical absorption coefficient is analyzed. The results reveal that the application of a magnetic field can increase the peak value of the absorption coefficient and cause a blue shift phenomenon. With the increase of light intensity, the peak splitting in total optical absorption appears. With the increase of the distance between the impurity and the center of the quantum ring, the spacing of the energy level decreases, resulting in a decrease in the peak value of the total absorption coefficients, and a red shift occurs. On the other hand, when the impurity is located between the inner and outer radius, the opposite effects appear as the impurity is far from the center of the quantum ring.

topics: donor impurity, magnetic field, refractive index changes, absorption coefficient

1. Introduction

Quantum dots have a limiting effect on space carriers, resulting in completely discrete energy level structures and discrete absorption spectra (in the band and between bands) [1, 2]. Low-dimensional semiconductor quantum dots such as quantum dots, quantum well wires, and quantum wells can be prepared by means of metal-organic chemical vapor deposition and molecular beam epitaxy [3]. Unique structures of energy levels are found in each shape of quantum dots which makes quantum dots have excellent optical properties.

Recently, with the rapid development of nanostructure technology, the quantum ring (QR) topic has found application in both experimental and theoretical fundamental research of photoelectric structure. It has also become a hot spot in the research of condensed matter and optoelectronics [4–10], which is why it is also used in optoelectronic devices such as lasers, photodetectors, and single photon sources [11]. Consequently, the optical properties of QRs structures have become focus of interest of condensed matter and applied physics [12–24].

The optical absorption properties in QR depend mainly on the carriers interaction, the impurity effect, the confinement potential, and the applied external field. For example, one investigated intersubband optical absorptions in QRs respectively with an exciton [12] and two electrons [13] with the effective-mass approximation in the presence of a magnetic field or an electric field. The optical properties in QR with both the confinement potential and the Aharonov–Bohm effect were also studied [14, 15]. The relative refractive index change and the absorption coefficient in the double δ-doped GaAs MIGFET-like structure [16] and parabolic two-dimensional QRs [17] have been investigated under the electric and magnetic field effects. Recently, one has explored the effects of hydrostatic pressure [18], hydrostatic pressure, and aluminum concentration [19], as well as spin-orbit coupling [20] on the intraband optical absorption properties in QR. The hydrogenic impurity-induced effect on the optical properties of low-dimensional semiconductor QRs have raised a lot of concern in some areas of applied physics [21–24].

The above-mentioned research results are mainly calculated using the variational procedure, the compact density-matrix approach, and the perturbation method. These methods focus on Hamiltonian problems consisting of simple-form kinetic energy terms or carrier motions not far from the harmonic region of the potential energy. However, if the carrier motion is far from the harmonic (equilibrium) quantum structure, the dynamics operators tend to become quite complex, e.g., when solving the high-energy states of the complex quantum structure, due to the difficulty of choosing suitable basis functions, and then the above methods become less applicable. In addition, due to the limitations of computational methods, most of the above theoretical works focus on analyzing the eigenstates of impurities situated in the QR center and the transition from the

ground state to the excited state. Fortunately, the finite-element method was proposed to solve the two-dimensional Schrödinger equation [25] and has been applied in sever al typical examples.

In this paper, within the effective mass approximation, the energies of the lowest and first excited states are calculated in a two-dimensional GaAs QR within a donor impurity under an applied magnetic field, using the finite element method proposed by [25]. We have studied the effect of the donor impurity-related linear and nonlinear optical properties on the impurity position, magnetic field strength, and incident optical intensity. The rest of this paper is organized as follows: the theoretical model is described in Sect. 2; in Sect. 3 the research results are analyzed and discussed; and finally the conclusions are presented in Sect. 4.

2. Theory and calculation

In this work, we assume that a donor impurity can be located at arbitrary positions. The electron is confined in a two-dimensional GaAs QR of the inner radius R_1, outer radius R_2, and width $d = R_2 - R_1$. A uniform magnetic field is applied along the plane (direction z) perpendicular to the two-dimensional QR (see Fig. 1). In the polar coordinate (r, φ) system, the effective mass Hamiltonian of an electron in QR is obtained as follows

$$H = \frac{1}{2m_e}\left(\boldsymbol{p} + \frac{e}{c}\boldsymbol{A}\right)^2 + V(r), \tag{1}$$

where $|e|$ and m_e are the electron charge and the effective mass, respectively; $\boldsymbol{p}$ is the momentum; $\boldsymbol{A} = \frac{1}{2}\boldsymbol{B} \times \boldsymbol{r}$ and $\boldsymbol{B} = B_z\boldsymbol{z}$ are the magnetic potential vectors; $r = \sqrt{x^2 + y^2}$ is the distance between the electron and the center of QR. In (1), $V(r) = V_h(r) + V_c(r)$ and it consists of the heterostructure confinement (i.e., the geometric confinement) and the Coulomb interaction between the donor impurity and the electron within the ring. In the infinite potential well model, the confining potential $V_h(r)$ is given by

$$V_h(r) = \begin{cases} 0, & R_1 < r < R_2, \\ \infty, & \text{elsewhere.} \end{cases} \tag{2}$$

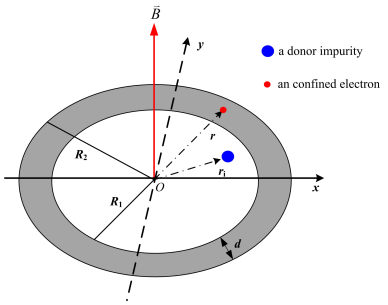

Fig. 1. Schematic diagram of QR under applied magnetic field; $R_1 = a^*$, $R_2 = 5a^*$ [26].

The Coulomb interaction potential $V_c(r)$ is written by

$$V_c(r) = -\frac{e^2}{\varepsilon\,|\boldsymbol{r} - \boldsymbol{r}_i|}, \tag{3}$$

where ε denotes the dielectric constant; $|\boldsymbol{r} - \boldsymbol{r}_i| = \sqrt{(x - x_i)^2 + (y - y_i)^2}$ is the distance between electron and impurity in two-dimensional GaAs QRs; x_i and y_i are the coordinates of impurity; $r_i = \sqrt{x_i^2 + y_i^2}$ is the distance between the impurity and the center of QR.

From (1), the Schrödinger equation obtained in the Cartesian coordinate system can be expressed as

$$\left[-\frac{\hbar^2}{2m_e}\nabla^2 + \frac{m_e\omega_m^2}{8}(x^2+y^2) + \frac{\hbar\omega_m}{2}\hat{L}_z + V(x,y)\right]\psi(x,y) = E\,\psi(x,y), \tag{4}$$

where $\omega_m = eB/(m_e c)$ is the electron cyclotron frequency, c is speed of light in vacuum, L_z is the projection of the electron angular momentum in the z direction.

When the impurity is located in the center of the quantum ring ($r_i = 0$), both $V_c(r)$ and $V_h(r)$ exhibit no dependence on the polar angle for a ring with cylindrical symmetry. From (4), Schrödinger equation can be obtained in polar coordinate system (r, φ), expressed as [26]

$$\left[-\frac{\hbar^2}{2m_e}\left(\frac{\partial^2}{\partial r^2} + \frac{\partial^2}{r\partial r} + \frac{\partial^2}{r^2\partial\phi^2}\right) - \frac{\mathrm{i}\hbar\omega_m}{2}\frac{\partial}{\partial\phi} + \frac{m_e\omega_m^2 r^2}{8} - \frac{e^2}{\varepsilon\, r} + V_c(r)\right]\psi(r,\phi) = E\,\psi(r,\phi). \tag{5}$$

For (5) the corresponding two-dimensional eigenstate $\psi(r, \phi)$ is given by the following formula

$$\psi(r,\phi) = \frac{1}{\sqrt{2\pi}}\,\mathrm{e}^{\mathrm{i}m\phi}\,R(r). \tag{6}$$

Substituting (6) into (5), we get the equation that only includes the radial wave function $R(r)$, as follows

$$\left[-\frac{\hbar^2}{2m_e}\frac{1}{r}\frac{\mathrm{d}}{\mathrm{d}r}\left(r\frac{\mathrm{d}}{\mathrm{d}r}\right) + \frac{\hbar^2}{2m_e}\frac{m^2}{r^2} + \frac{m_e}{8}\omega_m^2 r^2 + \frac{m}{2}\hbar\omega_m - \frac{e^2}{\varepsilon r}\right]R(r) = E_{nm}R(r). \tag{7}$$

Using $R_{\mathrm{B}} = m_e e^4/(2\pi^2\varepsilon^2)$ as energy unit, $a^* = \varepsilon\hbar^2/(m_e e)^2$ as a unit of length, (7) can be simplified as

$$\left[-\frac{1}{r}\frac{\mathrm{d}}{\mathrm{d}r}\left(r\frac{\mathrm{d}}{\mathrm{d}r}\right) + \frac{m^2}{r^2} + \frac{r^2}{16}\gamma^2 + \frac{m}{2}\gamma - \frac{2}{r} - E_{nm}\right]R(r) = 0, \tag{8}$$

where $\gamma = \hbar\omega_m/R_{\mathrm{B}}$ represents the magnetic field; $m = 0, \pm1, \pm2\ldots$ is the magnetic quantum number; n is the principal quantum number. For a given m, the energy levels E_{nm} and the wave function ψ_{nm} can be obtained by solving (8) with the use of the one dimensional finite element method.

When the impurity is distant from the center of the quantum ring, the Coulomb interaction potential $V_c(r)$ becomes related to the polar angle. In order to investigate the effect of the impurity position on the optical absorption properties, we consider $L_z = 0$. The Schrödinger equation (see (4)) is simplified as

$$\left[-\nabla^2+\frac{\gamma^2(x^2+y^2)}{16}-\frac{2}{\sqrt{(x-x_i)^2+(y-y_i)^2}}-E\right] \times\psi(x,y)=0. \quad (9)$$

The eigenvalue problem in (9) is solved by the two-dimensional finite element method.

This paper shows interesting results in the context of optical absorption of transitions from the lowest and first excited states. Assuming that the incident light radiation is polarized along the x-axis direction, the electric dipole transition matrix element between the lowest and first excited state is

$$M_{21} = \left|\langle\psi_2\left|r\cos(\varphi)\right|\psi_1\rangle\right|, \quad (10)$$

where $\Psi_1 = \Psi_{10}$ and $\Psi_2 = \Psi_{20}$ denote the wave functions of the lowest and first excited states, respectively.

The contributions of linear and third-order nonlinearity to the optical absorption coefficient and the refractive index changes are calculated using the compact density matrix method, Fermigen's rule, and iterative procedure. The analytical forms of the linear and third-order nonlinear optical absorption coefficients are obtained by [27, 28]

$$\alpha^{(1)}(\omega) = \omega\sqrt{\frac{\mu}{\varepsilon_r\varepsilon_0}}\,\frac{\rho\hbar\Gamma_{21}M_{21}^2}{\left(E_{21}-\hbar\omega\right)^2+\left(\hbar\Gamma_{21}\right)^2}, \quad (11)$$

and

$$\alpha^{(3)}(\omega,I) = \omega\sqrt{\frac{\mu}{\varepsilon_r\varepsilon_0}}\,\frac{2I\rho\hbar\Gamma_{21}M_{21}^4}{\varepsilon_0 nc\left[\left(E_{21}-\hbar\omega\right)^2+\left(\hbar\Gamma_{21}\right)^2\right]^2}, \quad (12)$$

where $E_{21} = E_2 - E_1$ is the energy difference between the lowest energy $E_2 = E_{20}$ and the first excited $E_1 = E_{10}$ energy state; μ denotes the permeability of the material; ρ is the electron charge density in QR; c is the speed of light in vacuum; ε_r is the relative dielectric constant of the medium, $n = \sqrt{\varepsilon_r}$ is the refractive index; $I = 2\varepsilon_0 nc|\boldsymbol{E}|^2$ is the incident light intensity; ε_0 is the dielectric constant in vacuum; $\Gamma_{21} = 1/\tau$ (τ is the relaxation time) is the decay rate from the first excited to lowest state; $\hbar\omega$ is the incident light intensity. Therefore, the total optical absorption coefficient is written as follows

$$\alpha\left(\omega,I\right) = \alpha^{(1)}\left(\omega\right) + \alpha^{(3)}\left(\omega,I\right). \quad (13)$$

In the same way, the expressions for linear and third-order nonlinear refractive index changes are defined as follows [27, 28]

$$\frac{\Delta n^{(1)}(\omega)}{n} = \frac{e^2\rho}{2n^2\varepsilon_0}\,\frac{\left(E_{21}-\hbar\omega\right)M_{21}^2}{\left(E_{21}-\hbar\omega\right)^2+\left(\hbar\Gamma_{21}\right)^2} \quad (14)$$

and

$$\frac{\Delta n^{(3)}(\omega,I)}{n} = \frac{e^4\rho\mu cI}{n^3\varepsilon_0}\,\frac{\left(E_{21}-\hbar\omega\right)M_{21}^4}{\left[\left(E_{21}-\hbar\omega\right)^2+\left(\hbar\Gamma_{21}\right)^2\right]^2}. \quad (15)$$

The total refractive index change is obtained as

$$\frac{\Delta n(\omega,I)}{n} = \frac{\Delta n^{(1)}(\omega)}{n} + \frac{\Delta n^{(3)}(\omega,I)}{n}. \quad (16)$$

3. Results and discussion

In this study, the following basic parameters are used for GaAs materials [27]: $\varepsilon = 13$, $\varepsilon_0 = 8.85\times10^{-12}$ F/m, $\rho = 5\times10^{22}$ m^{-3}, $\Gamma_{21} = 1/(0.14)$ ps^{-1}, $\mu = 1.256\times10^{-6}$ Tm/A, $n = 3.2$ and $m_e = 0.067\,m_0$ is the effective mass of the electron, where m_0 is the mass of the free electron. In the following study, the effective unit of dimension is $\alpha^* \approx 100$ Å, the effective unit of energy is $R_{\rm B} \approx 5.7$ meV.

Figure 2 describes the influence of different incident light intensity on the first-order, third-order and total absorption coefficients in QR when the impurity is situated in the center of QR and the magnetic field is $\gamma = R_{\rm B}$. As can be seen in Fig. 2, when the incident light intensity increases, the first-order absorption coefficient remains unchanged, and the peak appears at photon energy 13 meV. For the third-order absorption coefficient it increases with the increase of incident light intensity, and the minimum value appears at the photon energy 13 meV. The absorption coefficient decreases with the increase of incident light intensity. The incident light intensity increased, resulting in light absorption saturation. As the incident light intensity continues to increase, the peak absorption coefficient will split.

Figure 3 analyzes the effect of different incident light intensity on the first-order, third-order and total refractive index changes in QR with an impurity lied in the center of QR and the magnetic field is

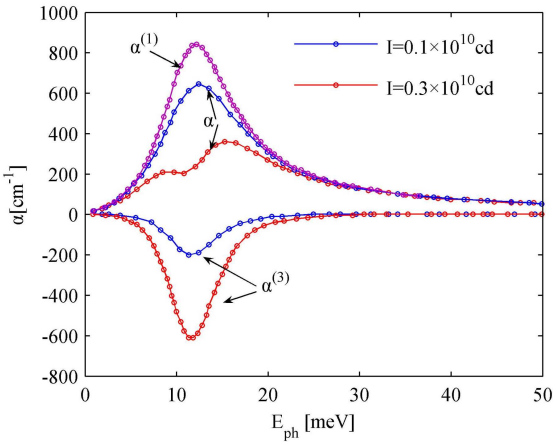

Fig. 2. The linear, third-order nonlinear and total absorption coefficient shown as photon energy $E_{\rm ph}$ with a donor impurity located at the center of the QR for different incident light intensities.

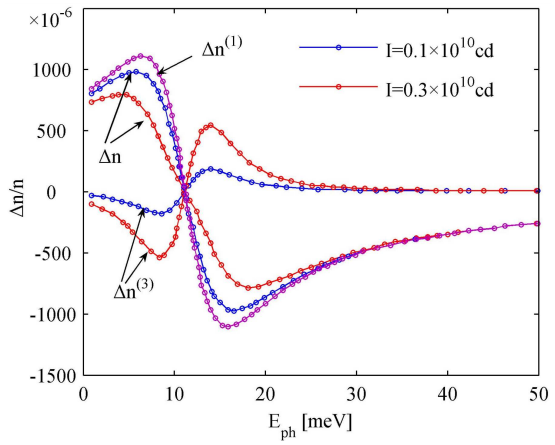

Fig. 3. The linear, third-order and total refractive index changes shown as photon energy $E_{\rm ph}$ with an impurity situated in the center of QR for different incident light intensities.

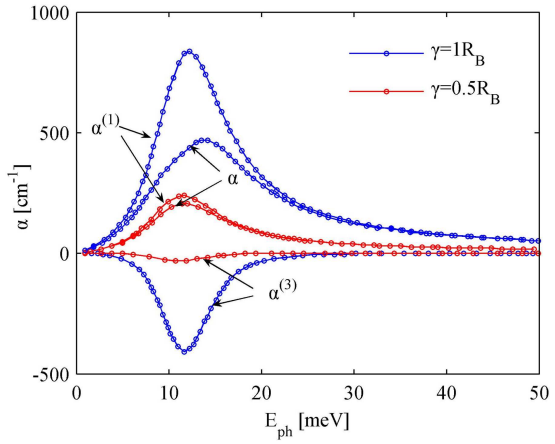

Fig. 4. The linear, third-order and total absorption coefficient as function of photon energy $E_{\rm ph}$ with a donor impurity lied in the center of QR for different magnetic fields.

$\gamma = R_{\rm B}$. As can be seen in Fig. 3, as the intensity I increases, the third-order nonlinear refractive index change decreases, while the linear refractive index change remains constant. The results show that the total refractive index change is reduced. We can see from these curves that the total refractive index changes decrease sharply with increasing photon energy between 6 and 15 meV. It is an anomalous dispersion phenomenon, defined as the absorption band due to the strong absorption of photons. The photon energy resonance peak corresponding to the total absorption coefficient in Fig. 2, corresponds to the point where the refractive index change curve intersects the horizontal axis. So the frequency of the energy is the resonance frequency of the system. In addition, in the region outside the anomalous dispersion, i.e., in the normal dispersion region, the refractive index smoothly increases with the increase of photon energy [22].

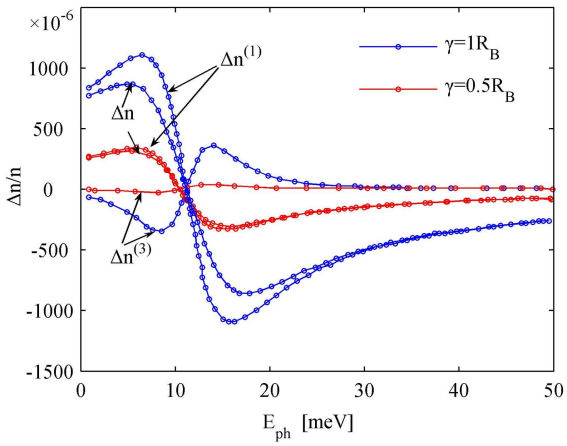

Fig. 5. The linear, third-order and total refractive index changes shown as photon energy $E_{\rm ph}$ with an impurity situated in the center of QR for different magnetic fields.

Figure 4 describes the effect of the magnetic field on the first-order, third-order and total absorption coefficient in QR with the impurity lied in the center and the incident light intensity $I = 0.2 \times 10^{10}$ cd. In Fig. 4, for the same light intensity, the first-order, the third-order and the total absorption coefficient increase with increasing magnetic field. The peak value of absorption coefficient moves to the right as the magnetic field increases, resulting in a blue shift phenomenon.

Figure 5 shows the changes of the first-order, third-order and total refractive index in QR as the photon energy when the impurity position lies in the center of QR and the incident light intensity is $I = 0.2 \times 10^{10}$ cd. Similarly, since the curves of the optical refractive index change with the incident light energy, the point where the curve intersects to the horizontal axis moves to the right with increasing magnetic field.

Figure 6 investigates the effect of impurities on the first-order, third-order and total absorption coefficient in QR, when the magnetic field is $\gamma = R_{\rm B}$ and the incident light intensity is $I = 0.2 \times 10^{10}$ cd. In Fig. 6, the position of the absorption peak moves to the left due to the appearance of impurities, which will lead to a red shift. To obtain the optical absorption peak, QR with impurities needs to absorb less photon energies, and the effect of the impurity can induce the increase of the absorption peak value.

Figure 7 analyzes the influence of impurities on the first-order, third-order and total refractive index changes in QR for $\gamma = R_{\rm B}$ and $I = 0.2 \times 10^{10}$ cd. From the curves showing the optical refractive index changes with the incident light energy, the point where the curves intersect with the horizontal axis moves to left when impurities appear. And the impurity effect induces an increase in the relative refractive index changes.

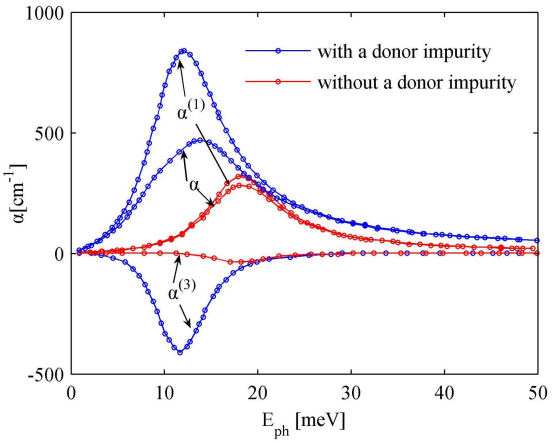

Fig. 6. Influence of impurities on the linear, third-order and total absorption coefficient with photon energy E_{ph}.

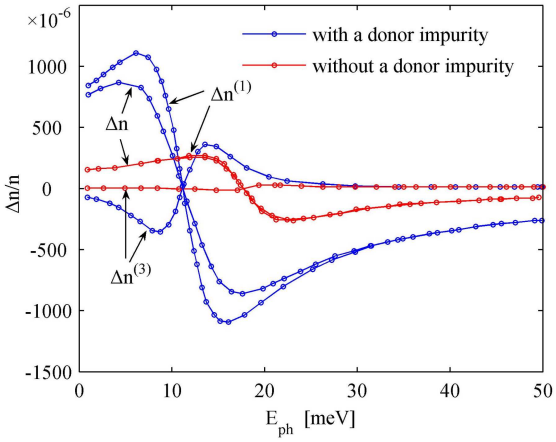

Fig. 7. The influence of impurity on the linear, the third-order and the total refractive index changes with photon energy E_{ph}.

Figure 8 depicts the electronic probability density of the lowest and first excited states when the impurities are located at different positions in the quantum ring. In Fig. 8, the impurity position has a significant effect on the electron probability density in the quantum ring. When the impurity is located at the center of the quantum ring, the probability density distribution $|\psi_1|^2$ of the lowest electron state has circular symmetry, and $|\psi_2|^2$ of the first excited state is symmetrical with respect to the axis diagonal of QRs. When the impurity positions are off from the center along the x-axis, in QRs all probability density functions are symmetrical about the x axis. The wavefunctions behaviors presented in Fig. 8 will be used in the following paragraphs for the analyses of light absorption coefficient and refractive index changes as a function of the impurity positions.

Figure 9 studies the influence of impurity position on the light absorption coefficient for $\gamma = 1 \times R_{\mathrm{B}}$ and $I = 0.2 \times 10^{10}$ cd, when the impurity positions

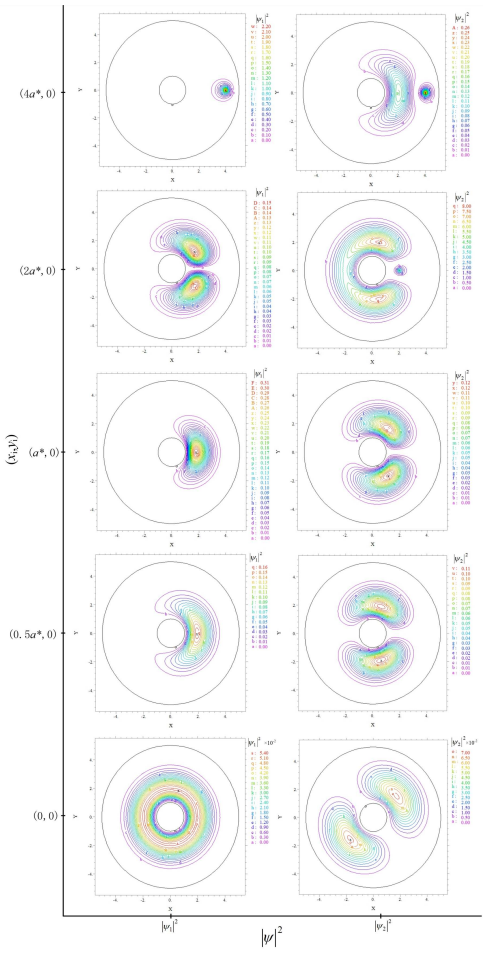

Fig. 8. The electronic probability density distribution of the lowest and first states when the impurities are located at different positions.

lie in the points $(0,0)$, $(0.5a^*,0)$, $(a^*,0)$, $(2a^*,0)$, and $(4a^*,0)$. As can be seen in Fig. 9, the impurity positions have a significant effect on the total light absorption coefficient. When the distance from the impurity position to the center is less than the inner radius ($r_i < R_1$), the value of absorption peak decreases significantly as the impurity is far from the center of QR. When the impurity is situated in the edge of the inner ring, i.e., $r_i = a^*$, the absorption peak value decreases more significantly. The incident photon energy corresponding to the value of the light absorption peak decreases as the distance of impurity from the QR center increases, so then the position of the absorption peak will move to the left, resulting in a red shift. When the impurities are located inside the quantum ring ($R_1 < r_i < R_2$), the absorption peak value begins to increase as the impurity is far from the center of QR. When the impurity approaches the edge of the outer ring (the impurity position at $(4a^*,0)$), the absorption peak value increases more significantly. The position of the absorption peak will move to the right as the impurity is away from the ring center, resulting in a blue shift. For example, at the impurity position $(2a^*,0)$, the

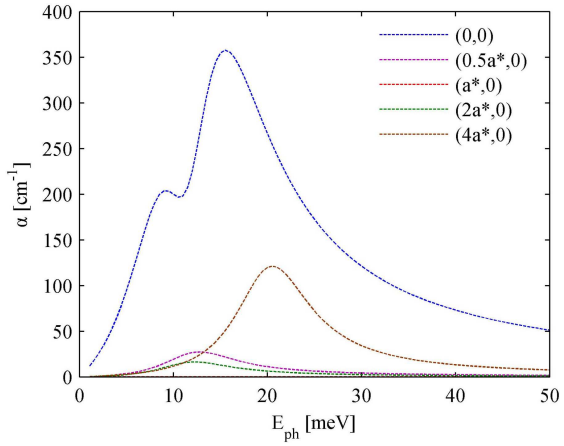

Fig. 9. The total light absorption coefficient shown as photon energy E_{ph} for impurities situated in different positions in QR.

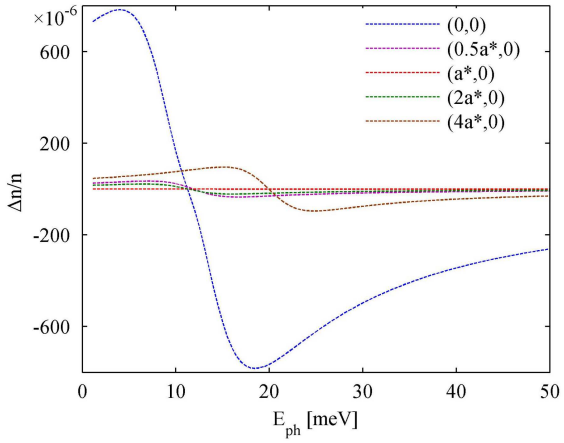

Fig. 10. The total refractive index changes shown as photon energy E_{ph} for impurities situated in different positions in QR.

incident photon energy corresponding to the light absorption peak is about 12 meV, while at the impurity position $(4a^*, 0)$, it is approximately 20 meV.

Figure 10 shows the total refractive index changes as a function of the photon energy when the impurity positions lie at the points $(0, 0)$, $(0.5a^*, 0)$, $(a^*, 0)$, $(2a^*, 0)$, and $(4a^*, 0)$, where $\gamma = R_{\mathrm{B}}$ and $I = 0.2 \times 10^{10}$ cd. In Fig. 10, there is a significant difference between $R_1 < r_i < R_2$ and $r_i < R_1$. For $r_i < R_1$, as the impurity distance from the center of QR increases, the total refractive index changes decrease and the region of anomalous dispersion defined as the absorption band gradually narrows. For example, for the impurity situated in the center of QR ($r_i = 0$), the total refractive index changes increase with the incident photon energy in the range 0–5 meV; while the total refractive index changes will decrease as the incident photon energy in the range of 5–16 meV. For the photon energy greater than 16 meV, the total refractive index changes increase again. When the distance between the position of the impurity and the ring center is $r_i = 0.5a^*$ compared with the impurity at the center, the total refractive index change is greatly reduced. When the impurity lies at the edge of the inner ring, i.e., $r_i = a^*$, the total refractive index change is almost zero. For $R_1 < r_i < R_2$, as the impurity distance from the center of QR increases, the total refractive index changes begin to increase, and the anomalous dispersion region gradually widens.

4. Conclusion

1. The total absorption coefficient decreases and splits as the incident light intensity increases continually for a given external magnetic field.
2. The light absorption coefficient and refractive index changes increases with increasing external magnetic field for a given incident light intensity. The obtained resonant peaks of the absorption coefficients need more photon energy, and the intersections of the optical refractive index change curves with the horizontal axis move to the right as the magnetic field increases, resulting in the blue shift phenomenon.
3. The existence of impurities does not affect the dependence of light absorption spectrum on the incident light intensity, but it can induce an increase of the absorption coefficient and the refractive index changes.
4. The impurity position has a significant effect on the optical absorption properties in QRs. When the impurity lies in the center of QR, the total optical absorption coefficient and refractive index changes are the largest. As the impurities are far away from the center, the total absorption coefficient and refractive index changes decrease at impurity positions $r_i < R_1$ or increase at impurity positions $R_1 < r_i < R_2$ significantly. There is an obvious red shift phenomenon at points $r_i < R_1$ or a blue shift phenomenon at points $R_1 < r_i < R_2$.

Acknowledgments

This study was financially supported by the Guiding Innovation Fund of Northeast Petroleum University of China (No. 2019YDL-17).

References

[1] K.B. Kim, S.N. Lee, Y.H. Kim, M. Kim, *Appl. Sci. Converg. Technol.* **29**, 4 (2020).

[2] T. Kazimierczuk, S. Nowak, J. Suffczyński, P. Wojnar, A. Golnik, J.A. Gaj, P. Kossacki, *Acta Phys. Pol. A* **112**, 2 (2007).

[3] M. Solaimani, *Solid State Sci.* **108**, 106386 (2020).

[4] D. Bejan, C. Stan, *Philos. Mag.* **101**, 16 (2021).

[5] S.H. Ha, J. Zhu, *J. Appl. Phys.* **128**, 3 (2020).

[6] K. Mohammad, A.S. Elsaid, H. Eshtiaq, Y.M. Hajj, *Chin. J. Phys.* **64,** 9 (2020).

[7] R. Sellami, A.B. Mansour, M.S. Kehili, A. Melliti, *Physica E* **126**, 9 (2021).

[8] R. Sellami, M.S. Kehili, A.B. Mansour, A. Melliti, *Opt. Quant. Electron.* **53**, 5 (2021).

[9] R.A. Escorcia, W. Gutiérrez, I.D. Mikhailov, *Appl. Surf. Sci.* **509** (2020).

[10] Z. Mierczyk, M. Zygmunt, M. Kaszczuk, M. Muzal, *Acta Phys. Pol. A* **124**, 3 (2013).

[11] N. Wang, W.H. Tian, H.S. Zhang, X.D. Yu, X.L. Yin, Y.G. Du, D.L. Li, *Acta Photon. Sin.* **49**, 9 (2020).

[12] W.F. Xia, *Opt. Commun.* **283**, 7 (2010).

[13] W.F. Xia, *Phys. Lett. A* **374**, 9 (2010).

[14] S.J. Liang, W.F. Xia, H.Y. Shen, *Opt. Commun.* **284**, 24 (2011).

[15] Z. Barticevic, G. Fuster, M. Pacheco, *Phys. Rev. B* **65**, 19 (2000).

[16] J.C. Martínez-Orozco, K.A. Rodríguez-Magdaleno, J.R. Suarez-Lopez A.C. Duque, R.L. Restrepo, *Superlattice Microst.* **92**, (2016).

[17] C.M. Duque, A.L. Morales, M.E. Mora-Ramos, A.C. Duque, *J. Lumin.* **143**, (2013).

[18] A. Kh. Manaselyan, M.G. Barseghyan, A.A. Kirakosyan, D. Laroze, C.A. Duque, *Physica E* **60**, 1 (2014).

[19] M. Fulla, J. Marín, W. Gutiérrez, C.A. Duque, M.E. Mora-Ramos, *Acta Phys. Pol. A* **125**, 2 (2014).

[20] V.N. Mughnetsyan, A.Kh. Manaselyan, M.G. Barseghyan, A.A. Kirakosyan, *J. Lumin.* **134**, (2013).

[21] S. Wang, Y. Kang, X.L. Li, *J. Semicond.* **37**, 11 (2016).

[22] C.M. Duque, R.E. Acosta, A.L. Morales, M.E. Mora-Ramos, R.L. Restrepo, J.K. Ojeda, C.A. Duque, *Opt. Mater.* **60**, (2016).

[23] R. Restrepo, J. Martínez-Orozco, M. Barseghyan, M.E. Mora-Ramos, C.A. Duque, *Acta Phys. Pol. A* **125**, 2 (2014).

[24] C.M. Duque, M.E. Mora-Ramos, C.A. Duque, *Opt. Commun.* **285**, 5456 (2012).

[25] N. Sat0, S. Iwata, *J. Comput. Chem.* **9**, 3 (1988).

[26] Y. Kang, S. Wang, X.L. Li, *J. Semicond.* **36**, 3 (2015).

[27] M. Sahin, *J. Appl. Phys.* **106**, 6 (2009).

[28] B. Cakir, Y. Yakar, A. Özmen, *J. Lumin.* **132**, 10 (2012).